

Research Article

Growth, structure refinement, thermal expansion and optical spectroscopy of Tm³⁺-doped MgMoO₄

Kirill Subbotin^{a,b}, Anatolii Titov^{a,b}, Denis Lis^b, Yulia Zimina^{a,b}, Yana Didenko^{a,b}, Ghassen Zin Elabedine^c, Kirill Eremeev^d, Rosa Maria Solé^c, Magdalena Aguiló^c, Pavel Volkov^e, Pavel Popov^f, Elena Chernova^a, Francesc Díaz^c, Patrice Camy^d, Pavel Loiko^d, Xavier Mateos^{c,*}¹

^a Prokhorov General Physics Institute, Russian Academy of Sciences, 38 Vavilova St., 119991 Moscow, Russia

^b Mendeleev University of Chemical Technology of Russia, 9 Miusskaya Sq, 125049, Moscow, Russia

^c Universitat Rovira I Virgili (URV), Física I Cristal·lografia de Materials (FiCMA), Marcel·lí Domingo 1, 43007, Tarragona, Spain

^d Centre de Recherche sur Les Ions, Les Matériaux et La Photonique (CIMAP), UMR 6252 CEA-CNRS-ENSICAEN, Université de Caen Normandie, 6 Boulevard Maréchal Juin, 14050, Caen Cedex 4, France

^e NRC "Kurchatov Institute" — IREA Shared Knowledge Center, Moscow, Russia

^f Petrovsky Bryansk State University, 14 Bezhitskaya St., 241023, Bryansk, Russia



ARTICLE INFO

Keywords:

Molybdates
Thulium ions
Czochralski method
Crystal structure
Raman spectra
Luminescence

ABSTRACT

Thulium-doped magnesium molybdate single-crystal (Tm³⁺:MgMoO₄) was grown by the Czochralski method (melting point: 1322 °C). The actual Tm³⁺ doping level was measured to be 0.1 at.% (the segregation coefficient was only 0.02). Tm:MgMoO₄ belongs to the monoclinic class (sp. gr. C2/m, lattice constants: $a = 10.2769(2) \text{ \AA}$, $b = 9.2898(5) \text{ \AA}$, $c = 7.0269(4) \text{ \AA}$, $\beta = 106.898(6)^\circ$). The thermal expansion tensor of this crystal is determined. Its thermal conductivity is also measured at 50–300 K (at room temperature, it amounts to $2.64 \text{ Wm}^{-1}\text{K}^{-1}$). Polarized Raman spectra are presented and the strongest mode is found at 957 cm^{-1} . Optical spectroscopy of Tm³⁺ ions is studied indicating broad emission bands extending beyond $2 \mu\text{m}$ (the ${}^3\text{F}_4 \rightarrow {}^3\text{H}_6$ transition) and a long lifetime of the ${}^3\text{F}_4$ excited-state (1.972 ms). This makes Tm:MgMoO₄ promising for broadly tunable and mode-locked lasers, when the technological problem of fabricating crystals with higher Tm³⁺ concentrations will be solved.

1. Introduction

Double tungstate and molybdate crystals containing the WO₄/MoO₄ groups are attractive laser host media for doping with trivalent rare-earth ions (RE³⁺) [1,2]. These crystals exhibit a great variety of structural types [3]. Among them, disordered tetragonal (sp. gr. I4₁/a) crystals NaR(XO₄)₂ [1] and ordered monoclinic (sp. gr. C2/c) crystals KR(XO₄)₂ [2] where R = Gd, Y, Lu and X = W/Mo are the most commonly used ones. In the past years, the crystal family of divalent metal monotungstates MWO₄ (where M = Mg, Zn, Mn, Cd, etc.), have attracted a lot of attention for RE³⁺ doping as well [4–6]. These crystals belong to the monoclinic class (sp. gr. P2/c) adopting the ordered wolframite-type structure [7,8].

One example: magnesium monotungstate crystal MgWO₄ which has

been recognized as an excellent host for doping with various RE³⁺ ions such as Yb³⁺ [4,9], Er³⁺ [10], Tm³⁺ [5,11] or Ho³⁺ [12] owing to (i) good thermal and thermo-mechanical properties of the host matrix, (ii) strong natural birefringence, (iii) intense and strongly polarized spectral bands of the dopant RE³⁺ ions; (iv) strong crystal fields leading to large Stark splitting of the RE³⁺ multiplets and broad emission bands [13] and (v) Raman activity. The high thermal conductivity of MgWO₄ ($8.7 \text{ Wm}^{-1}\text{K}^{-1}$ at room temperature [14]) makes it exceptional among other laser host crystals of the double tungstate/double molybdate families.

In particular, MgWO₄ crystals doped with thulium ions (Tm³⁺) exhibit broadband strongly polarized emission extending beyond $2 \mu\text{m}$ (the ${}^3\text{F}_4 \rightarrow {}^3\text{H}_6$ transition) [13]. Recently, highly efficient, low threshold and wavelength-tunable lasing [11,13] was demonstrated using Tm:MgWO₄ crystals. Furthermore, the first generation of sub-100 fs pulses

* Corresponding author.

E-mail address: xavier.mateos@urv.cat (X. Mateos).

¹ Serra Hünter Fellow.

from a bulk solid-state laser at $\sim 2 \mu\text{m}$ was demonstrated in 2017 using a Tm:MgWO₄ crystal [15]. Note that MgWO₄ crystals are grown by the Top-Seeded Solution Growth (TSSG) method (from the flux) [4,5].

The molybdate counterpart of MgWO₄ is also known, MgMoO₄ [16–18]. This crystal melts congruently and can be easily grown by the Czochralski (Cz) method. The structure of MgMoO₄ (Fig. 1) is different from that of MgWO₄, although it is also monoclinic. It belongs to the *C2/m* space group and the *2/m* point group, with the unit-cell parameters $a = 10.273(3)\text{\AA}$, $b = 9.288(3)\text{\AA}$, $c = 7.025(2)\text{\AA}$ and $\beta = 106.96^\circ$ [19]. The MgMoO₄ crystal shows a layered structure: the layers of two non-equivalent kinds of MgO₆ octahedra formed around Mg1 (Wyckoff: 4g) and Mg2 (Wyckoff: 4i) sites are separated by the layers of two non-equivalent kinds of MoO₄ tetrahedra. The neighbouring MgO₆ octahedra are connected by the shared edges. According to the structure refinement and EPR studies, the dopant RE³⁺ ions tend to replace for the host-forming cations Mg²⁺ in one of the lattice sites, namely, the Mg1 one [20,21]. This is because of the stronger distortion of the Mg1O₆ octahedra and longer Mg1 – O distances tolerating the difference in the ionic radii of VI-fold oxygen coordinated Mg²⁺ (0.72 Å) and, for example, Tm³⁺ (0.88 Å), as compared to almost ideal Mg2O₆ octahedra with shorter metal – oxygen interatomic distances.

The first successful attempts to grow MgMoO₄ single crystals by the Cz technique have been reported in 1963 [23], and in 1966 [24]. Later, the Cz technique has been successfully used for the growth of both undoped MgMoO₄ crystals [25–27], and crystals doped with Gd³⁺, Fe²⁺ [21], Yb³⁺ [25] and Nd³⁺ [28] ions. Cr³⁺ [16,18] and Yb³⁺ [29] doped MgMoO₄ single crystals have also been grown from K₂Mo₂O₇ [18,29] or Na₂MoO₄ + MoO₃ [16] fluxes, respectively.

The specific heat capacity and some other thermal properties of the MgMoO₄ crystal were measured in Refs. [18,30,31]. Various characteristics of flux-grown Cr³⁺:MgMoO₄ single crystals have been studied [18], including linear thermal expansion coefficients and some mechanical strength characteristics (micro-hardness, crack resistance) along the three crystallographic directions.

The optical and spectroscopic properties of undoped MgMoO₄ fabricated by various techniques have been extensively studied to the moment [17,22,25,32–35]. Some data on spectroscopic properties are also available in the literature for MgMoO₄ crystals doped with Cr³⁺ [16,18], Yb³⁺ [25,29], Nd³⁺ [28], Eu³⁺ [36,37], Eu³⁺, Dy³⁺ [38], and Eu³⁺, Bi³⁺ ions [20]. Similar to most of the other molybdate crystals, undoped MgMoO₄ possesses its own broadband luminescence in the visible range under UV or X-ray excitation, as well as by electron beam or α -particles [17,22,25,32–35,37] due to the charge-transfer transition with the formation/recombination of self-trapped excitons at the [MoO₄] clusters [12,25,34,39], moreover, luminescence due to deep traps at point defects or oxygen vacancies in the [MoO₄] clusters [15,35]. Besides the luminescence decay, the excited-state energy can be easily transferred to the RE³⁺ dopants (e.g., Eu³⁺, Yb³⁺) with the subsequent luminescence through the above-mentioned centers [25,37]. Hence, this material is

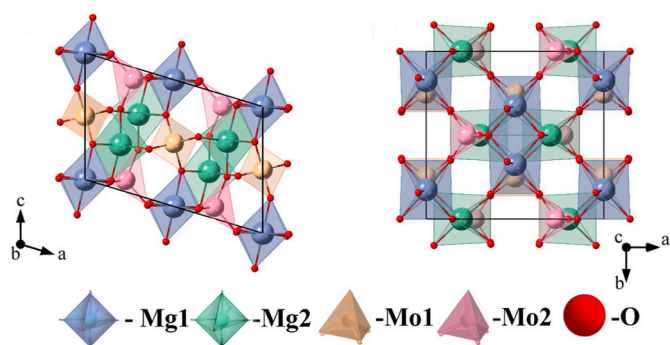


Fig. 1. The structure of MgMoO₄ in two crystallographic projections (according to Ref. [22]), black lines – unit-cell.

interesting for applications as scintillators [8,25], phosphors [11,33,37] and laser hosts [18]. Besides that, the MgMoO₄ powder is widely used as a catalyst for dehydrogenation of saturated hydrocarbons [40,41].

Meanwhile, no report on the growth nor studies of Tm³⁺-doped MgMoO₄ crystals can be found in the literature. In the present work, we report on the successful Czochralski growth, as well as the structural, thermal and spectroscopic investigations of both undoped and Tm³⁺-doped MgMoO₄ single crystals.

2. Experimental

2.1. Crystal growth

The single-crystals of MgMoO₄ and Tm:MgMoO₄ were grown by the Cz method at the “Kristall-2” growth machine (USSR) in air using a Pt/Rh crucible with a diameter/height of $\Phi 30$ mm/30 mm, respectively, and a [001] oriented seed cut from an undoped MgMoO₄ single crystal. The raw materials were MgO (purity: 4 N, Krasnyi Khimik, USSR), MoO₃ (4 N, Lankhit Ltd., Russia), and Tm₂O₃ (4 N, USSR). The Tm³⁺ content in the initial melt for the growth of Tm:MgMoO₄ was 5 at.% with respect to Mg²⁺ ions. No charge compensators were used.

Prior to melting, the blend of the initial chemicals was thoroughly mixed and calcined at 700 °C during 5 h (h) for solid-phase synthesis. Without calcining, a substantial part of MoO₃ would evaporate from the melt as the saturated vapor pressure of unbound MoO₃ at the MgMoO₄ melting point (1322 °C, see below) exceeds 1 atm.

The pulling rate/rotation speed were 1 mm/h and 6 revolutions per minute (rpm), respectively. When the growth was completed, the crystals were slowly cooled down to room temperature (RT, 20 °C) at a rate of 8 °C/h to reduce the risk of crystal cracking. Then, the crystals were additionally annealed in air at 800 °C for 2 weeks.

2.2. Characterization methods

The actual Tm³⁺ concentration in the MgMoO₄ crystal was measured by inductively coupled plasma atomic emission spectroscopy (ICP–AES) using an iCAP6300 duo Thermo Fisher Scientific spectrometer. Before the measurement, a piece of the crystal was thoroughly ground into powder and dissolved in H₃PO₄ (Suprapur, Merck) at a temperature of 400 °C.

Another piece of the as-grown crystal was ground into powder for X-ray powder diffraction (XRD) analysis. These measurements were carried out using a Bruker-AXS D8-Advance diffractometer with a vertical θ - θ goniometer and Cu K α radiation. The detection of the diffracted X-rays was made with a LynxEye-XE-T PSD detector with an opening angle of 2.94°. The data were collected in the 2θ interval from 5 to 90°, with step size of 0.02° and step time of 2 s. The measured XRD pattern was refined by the Rietveld method using the Topas V6 software. The crystal structure of undoped MgMoO₄ (PDF #72–2153, ICSD database) [19] was used as the initial model for the Rietveld refinement. XRD measurements at elevated temperatures, from RT to 650 °C, were performed to calculate the linear thermal expansion coefficients. The same diffractometer was used with the same step size/time, and the measurements were made in the 2θ range from 5 to 80°. A delay of 300 s was applied before each measurement. The crystal to be used for optical characterization was oriented in the crystallographic frame using single-crystal X-ray diffraction.

The differential thermal analysis (DTA) from RT to 1400 °C, in heating and cooling processes, was performed using a TA Instruments SDT 2960 equipment. The measurements were carried out in Pt crucibles and Al₂O₃ was used as a reference material. The heating and cooling rates were 10 °C/min, under a nitrogen flow of 140 cm³/min.

The thermal conductivity of undoped MgMoO₄ was measured by the method of stationary longitudinal heat flow in the temperature range of 50–300 K using an [001]-oriented crystal. To ensure a plane shape of the isothermal surfaces, the resistive heater was glued to the end surface of

the sample. The measurement error did not exceed $\pm 6\%$. More details can be found elsewhere [42].

The polarized Raman spectra were measured for a [010]-cut crystal using a confocal laser microscope (InVia, Renishaw) equipped with a $\times 50$ Leica objective and an Ar^+ ion laser (514 nm). The unpolarized absorption spectra were measured using a Varian Cary 5000 spectrophotometer. The polarized luminescence spectra were measured using a Glan-Taylor polarizer and an optical spectrum analyzer (AQ6376, Yokogawa) with a ZrF_4 fiber. The luminescence decay was studied using a ns optical parametric oscillator (Horizon, Continuum), a 1/4 m monochromator (Oriol 77,200), an InGaAs detector and an 8 GHz digital oscilloscope (DSA70804B, Tektronix).

3. Results and discussion

3.1. Grown crystals

The photographs of the as-grown MgMoO_4 and Tm:MgMoO_4 crystals are shown in Fig. 2. Both crystals exhibited a bright saffron-yellow coloration, with a maximum diameter of ~ 15 – 16 mm and a length of ~ 40 – 50 mm. The boules demonstrated a highly expressed natural faceting. Besides that, the Tm:MgMoO_4 crystal contained a couple of cleavage cracks. Spasskii et al. identified one of the cleavage planes of MgMoO_4 as $\{9\ 11\ 0\}$ [25]. The cracks were flat and nearly perpendicular to each other confirming the identification of the cleavage planes proposed in Ref. [25].

During the growth of magnesium molybdate crystals, a pronounced volatility of MoO_3 from the surface of the melt was observed. The vapor then condensed at cold elements of the growth zone (i.e., the heat insulating ceramics, the upper parts of the seed holder) as needle-shaped yellow crystallites. Such volatility has been discussed previously [18,29] and it can result in the formation of molybdenum vacancies in the grown crystals. On the other hand, the usage of a single-crystalline MgMoO_4 seed under such circumstances may be considered as if it experiences annealing in MoO_3 vapor atmosphere. We have observed that after the usage of a MgMoO_4 seed in several crystal growth processes, its coloration step-by-step changed from saffron-yellow to pale yellowish, almost colorless one. This motivated us to study the absorption of such samples.

Fig. 3 shows the absorption spectra of an undoped MgMoO_4 crystal before and after its usage as a seed for further molybdate crystal growth. The as-grown crystal exhibits rather strong and broad absorption band



Fig. 2. Photographs of the as-grown crystal boules of (a) undoped MgMoO_4 and (b) 0.1 at.% Tm^{3+} -doped MgMoO_4 (actual doping level). The growth direction is along the [001] axis.

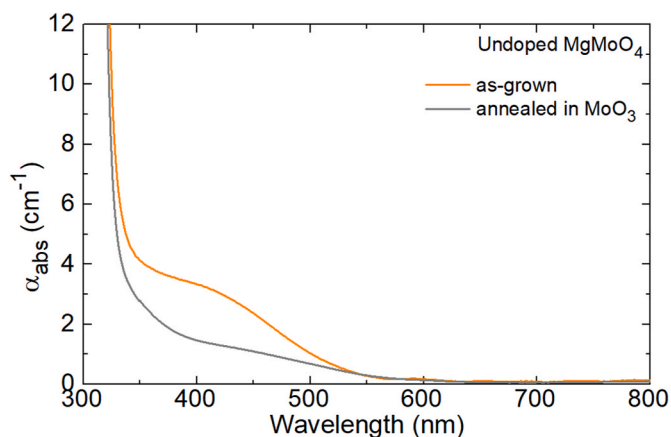


Fig. 3. Unpolarized absorption spectra of the as-grown MgMoO_4 crystal, and a seed cut from this crystal after its annealing in the MoO_3 vapor atmosphere, inset – photograph of the polished crystal plates (left – cut from an as-grown crystal, right – after annealing).

centered at ~ 430 nm, which causes the saffron-yellow coloration. After the usage as a seed (annealing in MoO_3 vapor atmosphere), the intensity of this absorption band drastically decreased, although, it did not disappear completely. This indicates that the concentration of the corresponding vibronic color centers in the crystal was substantially reduced after such an annealing. Note that annealing of the same crystal in air does not lead to the same effect indicating that the observed color centers are related with molybdenum deficiency.

The coloration of scheelite-type double molybdate crystals was analyzed previously [43], including the saffron-yellow one which appeared sometimes in such crystals after their annealing in air. It was concluded that such coloration is caused by a hole center at the molybdenum vacancy. It seems that similar color centers are also formed in the MgMoO_4 crystals, while the annealing in MoO_3 vapor atmosphere eliminates them.

The actual Tm^{3+} concentration in the Tm:MgMoO_4 crystal was measured to be 0.096 at.% with respect to Mg^{2+} corresponding to an ion density $N_{\text{Tm}} = 0.13 \times 10^{20} \text{ cm}^{-3}$. According to the ratio between the actual dopant concentration in the crystal and its nominal concentration in the initial melt, the Tm^{3+} segregation coefficient was determined, $K_{\text{Tm}} = 0.02$. Previously, the segregation coefficient of Nd^{3+} in MgMoO_4 was also determined to be rather low, $K_{\text{Nd}} < 0.01$ [28].

Such a low value is typical for RE^{3+} dopant ions in Mg^{2+} -containing crystals. For example, the Yb^{3+} segregation coefficient between the Mg_2SiO_4 crystal and the melt is as low as 0.0009 [44]. It is due to the heterovalent character of the $\text{Mg}^{2+} \rightarrow \text{Tm}^{3+}$ substitution, as well as the essential difference in the ionic radii of these cations, namely 0.72 Å (Mg^{2+}) and 0.88 Å (Tm^{3+}) for VI-fold oxygen coordination. We believe that the choice of a proper charge compensator may substantially increase the segregation coefficient of Tm^{3+} ions in MgMoO_4 . Indeed, according to the previous studies, the usage of a proper amount of Li^+ charge compensator doubles the Yb^{3+} segregation coefficient in Yb^{3+} , $\text{Li}^+:\text{ZnWO}_4$ crystals as compared to singly Yb^{3+} -doped ones [45], whereas the usage of Nb^{5+} charge compensator raises the Nd^{3+} segregation coefficient in $\text{Nd}^{3+}, \text{Li}^+:\text{CaMoO}_4$ by an order of magnitude (up to almost unity) in comparison with solely Nd^{3+} -doped CaMoO_4 crystals [46].

3.2. Crystal structure

Two polymorphs of MgMoO_4 are known. The α -phase possesses a cuproscheelite-type structure (sp. gr. $P-1$), similar to CuMoO_4 and $\alpha\text{-ZnMoO}_4$ [47]. The β -phase adopts the monoclinic structure (sp. gr. $C2/m$) and it is isostructural to the high-temperature phase of

α -MnMoO₄ [48].

Fig. 4(a) shows the measured X-ray powder diffraction pattern of the as-grown 0.1 at.% Tm:MgMoO₄ crystal together with the theoretical pattern of undoped magnesium molybdate (ICSD card No. 72–2153), and Miller's indices (*hkl*) for intense diffraction peaks. Tm:MgMoO₄ belongs to the monoclinic class (β -phase, sp. gr. C_{2h}³ - C2/m, No. 12, point group 2/m) and it is isostructural to undoped β -MgMoO₄. The inspection of the XRD pattern reveals no other phases except the monoclinic one. Fig. 4(b) shows the Rietveld refinement plots for 0.1 at.% Tm:MgMoO₄ (measured, calculated, and residual profiles), with vertical dashes indicating Bragg reflections. The actual Tm³⁺ doping level measured by ICP-AES was used to determine the occupancy factors of the Mg1 (Wyckoff: 4g) site. It was assumed that the dopant ions enter exclusively into these sites [20,21]. The refined lattice constants are $a = 10.2769(2)$ Å, $b = 9.2898(5)$ Å, $c = 7.0269(4)$ Å and $\beta = \alpha^{\wedge}c = 106.898(6)^{\circ}$ (the number of formula units in the unit-cell: $Z = 8$), the volume of the unit-cell $V = 641.902(7)$ Å³ and the calculated crystal density ρ_{calc} of 3.888 g/cm³. The determined lattice parameters are slightly larger than those for undoped β -MgMoO₄ powders reported in Refs. [19,39]. The calculated pattern well matched the experimental one and the refinement converged as indicated by the reliability factors, $R_p = 4.93\%$, $R_{\text{wp}} = 8.10\%$ and $R_{\text{exp}} = 2.61\%$ (the reduced chi-squared: $\chi^2 = (R_{\text{wp}}/R_{\text{exp}})^2 = 9.61$). The fractional atomic coordinates, site occupancy factors and isotropic displacement parameters attained in the Rietveld refinement

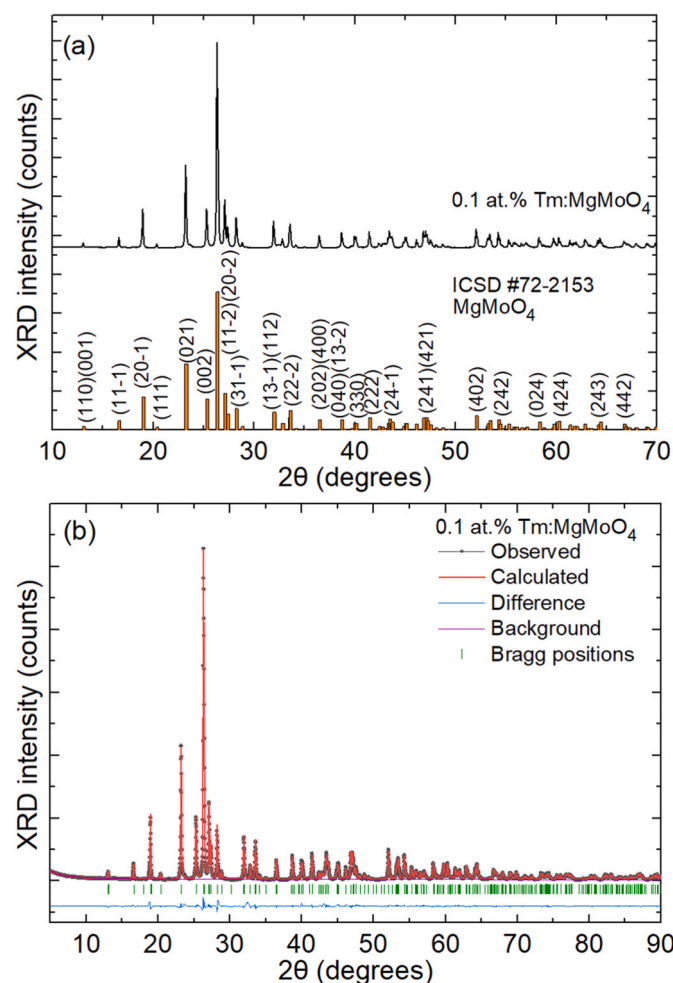


Fig. 4. X-ray powder diffraction (XRD) study of the 0.1 at.% Tm:MgMoO₄ crystal: (a) measured XRD pattern, the theoretical pattern for MgMoO₄ (ICSD card No. 72–2153 is shown for comparison), *numbers* – Miller's indices, (*hkl*); (b) Rietveld refinement plots: measured, calculated, and residual profiles, *vertical dashes* – Bragg reflections.

are listed in Table 1.

The metal – to – oxygen (Mg – O and Mo – O) interatomic distances are listed in Table 2. The corresponding polyhedra [Mg1O₆], [Mg2O₆], [Mo1O₄] and [Mo2O₄] are drawn in Fig. 5.

3.3. DTA analysis

The DTA analysis of the Tm:MgMoO₄ crystal performed in the temperature range of 20–1400 °C revealed only one sharp thermal effect at 1322 °C corresponding to congruent melting/crystallization, see Fig. 6. This value nearly coincides with that reported in Ref. [49] for undoped MgMoO₄, 1320 °C.

3.4. Thermal expansion

According to the results of the performed high-temperature XRD analysis of the Tm:MgMoO₄ crystal, Fig. 7, the linear thermal expansion tensor a_{ij} has been constructed in the crystallo-physical frame $\{X_1, X_2, X_3\}$, where $X_1 \parallel a$, $X_2 \parallel b$ and $X_3 \parallel c^*$, where c^* is the axis orthogonal to the a -axis and lying in the a - c plane:

$$(a_{ij}) = \begin{pmatrix} 7.089 & 0 & 0.222 \\ 0 & 14.30 & 0 \\ 0.222 & 0 & 3.706 \end{pmatrix} \times 10^{-6} \text{ K}^{-1}. \quad (1)$$

The tensor was then diagonalized to find the eigen-frame of thermal expansion $\{X_1', X_2', X_3'\}$ and the corresponding diagonal tensor elements. The eigen-frame orientation is: the X_1' axis is rotated at an angle of 3.74° from the a axis clockwise, the X_2' axis is parallel to the b axis and the X_3' axis is rotated at an angle of 13.16° from the c axis (anticlockwise), with the b axis pointing towards the observer. In this coordinate system, the linear thermal expansion tensor of Tm:MgMoO₄ is:

$$(a'_{ij}) = \begin{pmatrix} 7.103 & 0 & 0 \\ 0 & 14.30 & 0 \\ 0 & 0 & 3.691 \end{pmatrix} \times 10^{-6} \text{ K}^{-1}. \quad (2)$$

Our results reasonably agree with the previous report on the linear thermal expansion coefficients of a Cr:MgMoO₄ crystal measured by the dilatometry method along the three crystallographic axes: $\alpha_a = 10.10 \times 10^{-6} \text{ K}^{-1}$, $\alpha_b = 12.26 \times 10^{-6} \text{ K}^{-1}$ and $\alpha_c = 3.71 \times 10^{-6} \text{ K}^{-1}$ [18].

3.5. Thermal conductivity

The thermal conductivity κ of the undoped MgMoO₄ crystal was measured along the [001] direction in the temperature range of 50–300 K. It monotonously decreases with temperature, from 19.51 to 2.64 Wm⁻¹K⁻¹, as shown in Fig. 8. A similar behavior has been observed recently for ZnWO₄ and CdWO₄ crystals [50]. The thermal conductivity of MgMoO₄ at 300 K is only slightly lower than that of ZnWO₄ ($\kappa = 3.2 \text{ Wm}^{-1}\text{K}^{-1}$ along the [010] direction [50]) and is greatly reduced as compared to that of MgWO₄ ($\kappa = 8.7 \text{ Wm}^{-1}\text{K}^{-1}$ along arbitrary direction [14]).

3.6. Raman spectra

For the monoclinic β -phase of MgMoO₄, there are 8 molecules per unit cell. The group theory analysis predicts the following set of irreducible representations of the factor group C_{2h} in the center of the Brillouin zone ($\mathbf{k} = 0$): $\Gamma = 19A_g + 17B_g + 14A_u + 19B_u$ (optical modes) [48,51]. The even (*gerade*) modes (A_g and B_g) are Raman-active and uneven (*ungerade*) one (A_u and B_u) are IR-active. Among the Raman-active modes, 18 modes ($11A_g + 7B_g$) are the internal ones of the [MoO₄]²⁻ tetrahedral: symmetric stretching ($\nu_1, 2A_g$), anti-symmetric stretching ($\nu_3, 3A_g + 3B_g$), symmetric bending ($\nu_2, 3A_g + 1B_g$), and anti-symmetric stretching ($\nu_4, 3A_g + 3B_g$).

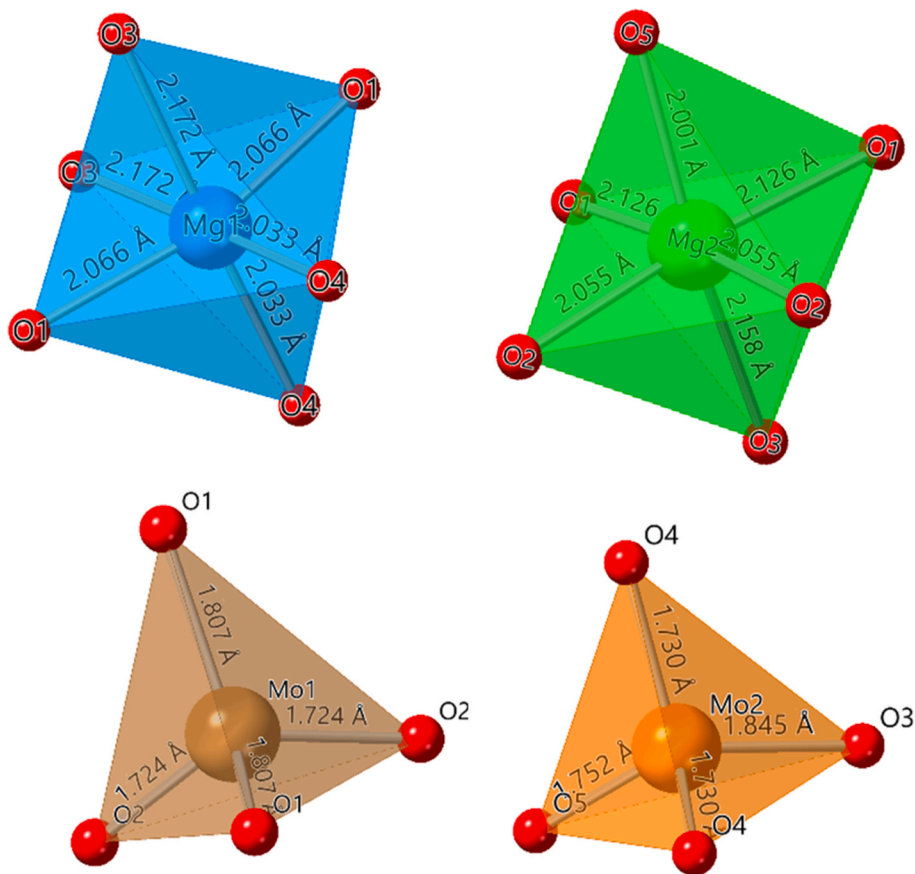
The polarized Raman spectra of a b -cut Tm:MgMoO₄ crystal are shown in Fig. 9. Here, Porto's notations are used. The Raman spectra

Table 1Fractional atomic coordinates (x/a , y/b , z/c), site occupancy factors (O.F.) and isotropic displacement parameters (B_{iso}) for 0.1 at.% Tm:MgMoO₄.

Atoms	x/a	y/b	z/c	O.F.	B_{iso} , Å ²	Wyckoff	Symmetry
Mg1	1/2	0.1791(3)	0	0.998	1.661(9)	4g	2
Tm	1/2	0.1791(3)	0	0.002	1.661(9)	4g	2
Mg2	0.7981(3)	1/2	0.6398(5)	1	0.056(7)	4i	<i>m</i>
Mo1	1/2	0.2523	1/2	1	0.105(6)	4h	2
Mo2	0.5433(2)	1/2	0.0955	1	0.068(4)	4i	<i>m</i>
O1	0.2121(3)	0.1505(9)	0.3088(9)	1	0.658(3)	8j	1
O2	0.3603(3)	0.3598(4)	0.3765(4)	1	1.182(3)	8j	1
O3	0.8552(6)	1/2	0.9577(8)	1	0.862(2)	4i	<i>m</i>
O4	0.6351(1)	0.3437(7)	0.0301	1	0.063(7)	8j	1
O5	0.2963(1)	0	0.3558(2)	1	0.294(7)	4i	<i>m</i>

Table 2Selected interatomic (metal – oxygen) distances for 0.1 at.% Tm:MgMoO₄.

[Mg1O ₆]	Å	[Mg2O ₆]	Å	[Mo1O ₄]	Å	[Mo2O ₄]	Å
Mg1–O1	2.066	Mg2–O1	2.126	Mo1–O1	1.807	Mo2–O3	1.845
Mg1–O1	2.066	Mg2–O1	2.126	Mo1–O1	1.807	Mo2–O4	1.730
Mg1–O3	2.172	Mg2–O2	2.055	Mo1–O2	1.724	Mo2–O4	1.730
Mg1–O3	2.172	Mg2–O2	2.055	Mo1–O2	1.724	Mo2–O5	1.752
Mg1–O4	2.033	Mg2–O3	2.158				
Mg1–O4	2.033	Mg2–O5	2.001				

**Fig. 5.** [Mg1O₆], [Mg2O₆], [Mo1O₄] and [Mo2O₄] polyhedra for the 0.1 at.% Tm:MgMoO₄ crystal.

contain intense peaks within two distinct ranges, 122–424 cm⁻¹ and 754–969 cm⁻¹, which is a typical behavior for monoclinic tungstate/molybdate crystals. The peaks from the low-frequency band are due to the lattice vibrations and some bending modes (ν_2 and ν_4) mixed with the lattice vibrations. The peaks from the high-frequency band are due to the stretching (ν_1 and ν_3) vibrations of the MgMoO₄ tetrahedra. The most intense mode appears at 957 cm⁻¹ and the highest phonon energy

is 969 cm⁻¹. Both these peaks are due to symmetric stretching (ν_1 , 2A_g) vibrations. Their peak linewidths (FWHM) are ~6 cm⁻¹.

3.7. Optical spectroscopy of Tm³⁺ ions

Due to the weak absorption of Tm³⁺ ions in a low-doped Tm:MgMoO₄ crystal, only the unpolarized optical absorption spectrum of

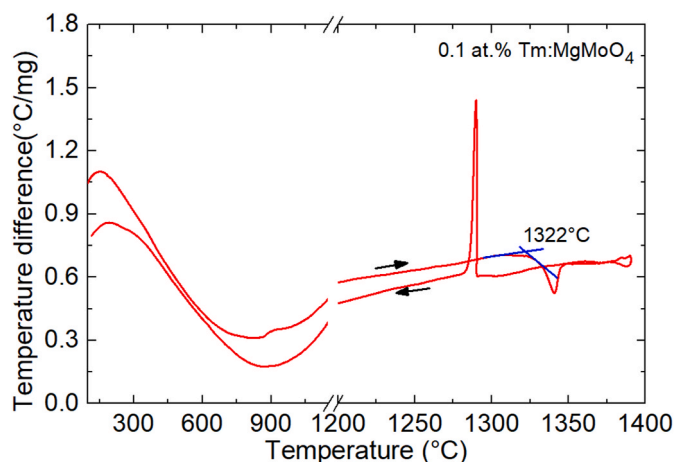


Fig. 6. Differential thermal analysis (DTA) curve for the 0.1 at.% Tm:MgMoO₄ crystal.

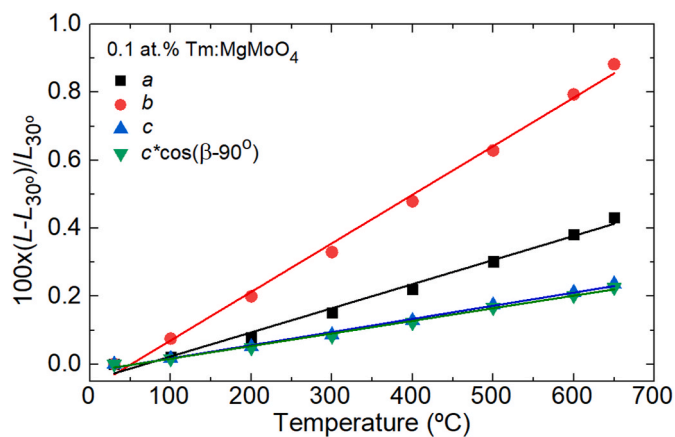


Fig. 7. Evolution of the lattice parameters of 0.1 at.% Tm:MgWO₄ with temperature.

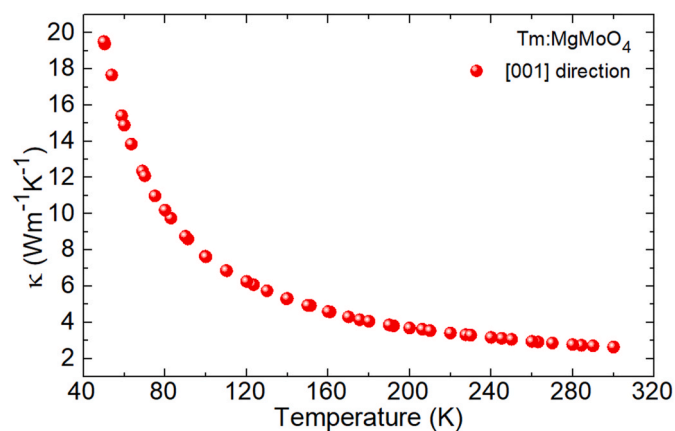


Fig. 8. Thermal conductivity of undoped MgMoO₄ along the [001] direction as a function of temperature.

the as-grown crystal was measured, Fig. 10. Here, the absorption bands are due to transitions of Tm³⁺ ions from the ground-state (³H₆) to the excited-states ³F₄ (~1.63 μm), ³H₅ (~1.21 μm), ³H₄ (~0.79 μm) and ³F_{2,3} (~0.68 μm). The broad absorption bands in the visible and near-IR underlying the Tm³⁺ bands are due to the above-mentioned color centers. They can be eliminated by annealing. Such bands are found at

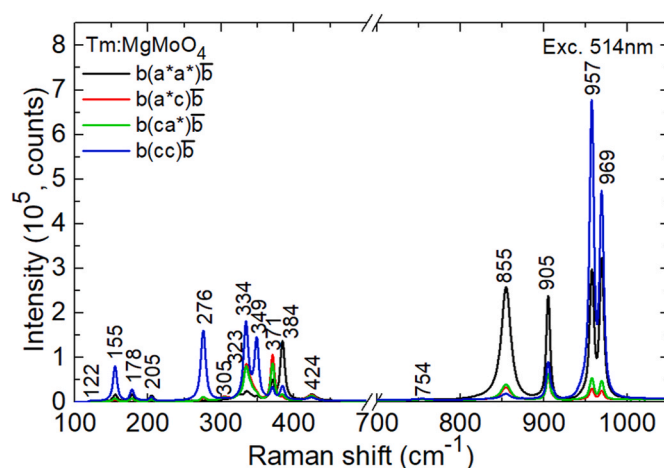


Fig. 9. Polarized Raman spectra of a [010]-cut 0.1 at.% Tm:MgMoO₄ crystal, λ_{exc} = 514 nm, numbers – Raman frequencies in cm⁻¹.

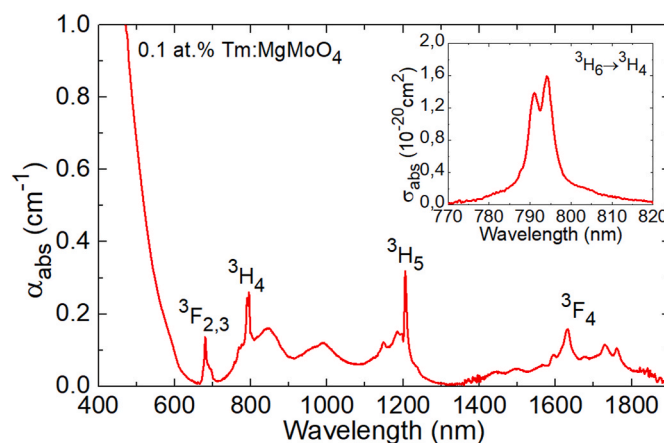


Fig. 10. Unpolarized absorption spectrum of the 0.1 at.% Tm:MgMoO₄ crystal, inset – absorption band corresponding to the ³H₆ → ³H₄ Tm³⁺ transition.

~590, 850 and 990 nm. For the ³H₆ → ³H₄ Tm³⁺ transition which is usually used for optical pumping, e.g., by commercial AlGaAs laser diodes, the calculated absorption cross-section σ_{abs} = α_{abs}/N_{Tm} is 1.60 × 10⁻²⁰ cm² at 794.2 nm (α_{abs} – absorption coefficient) corresponding to an absorption bandwidth (full width at half maximum, FWHM) of 6.6 nm. This value is broader than that for scheelite-type molybdates, e.g., ~5 nm for Tm:NaLa(MoO₄)₂ [52].

Under excitation at 794 nm (the ³H₆ → ³H₄ absorption band), Tm³⁺ ions in MgMoO₄ exhibit a broad and smooth emission band spanning from 1.6 up to 2.15 μm related to the ³F₄ → ³H₆ transition, Fig. 11. The luminescence spectra are strongly polarized, with the highest emission intensity corresponding to light polarization *E* || *a** and medium intensity – to *E* || *b*. They extend well beyond 2 μm (e.g., the long-wave emission peaks at which laser operation is expected are found at ~2000 nm and ~2050 nm) thus avoiding the structured water vapor absorption in air. This feature makes Tm:MgMoO₄ promising for generation of ultrashort (fs) pulses from mode-locked lasers.

The luminescence decay curve from the ³F₄ state of Tm³⁺ ions in MgMoO₄ was measured under resonant excitation at 1640 nm (the ³H₆ → ³F₄ absorption band). It is nearly single-exponential, see Fig. 12. It indicates that Tm³⁺ ions are located mostly in one of the two non-equivalent Mg²⁺ sites of the structure, in agreement with the conclusion made previously based on EPR studies for other RE³⁺ ions [20,21]. Another possibility is that for both sites, the Tm³⁺ ions show close transition probabilities. The measured luminescence lifetime of the ³F₄

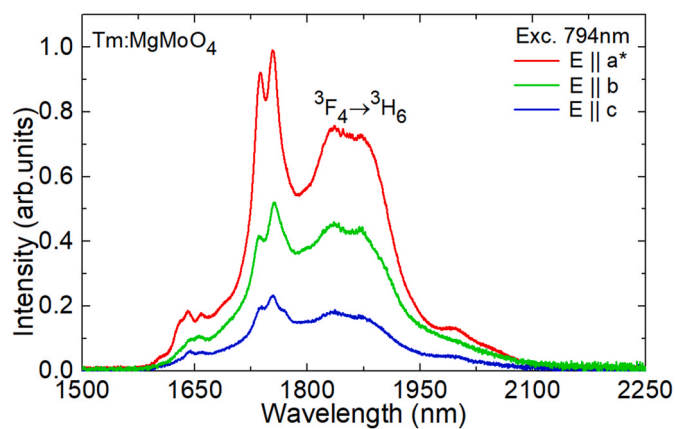


Fig. 11. Polarized luminescence spectra of Tm^{3+} ions in MgMoO_4 (the ${}^3\text{F}_4 \rightarrow {}^3\text{H}_6$ transition), $\lambda_{\text{exc}} = 794$ nm.

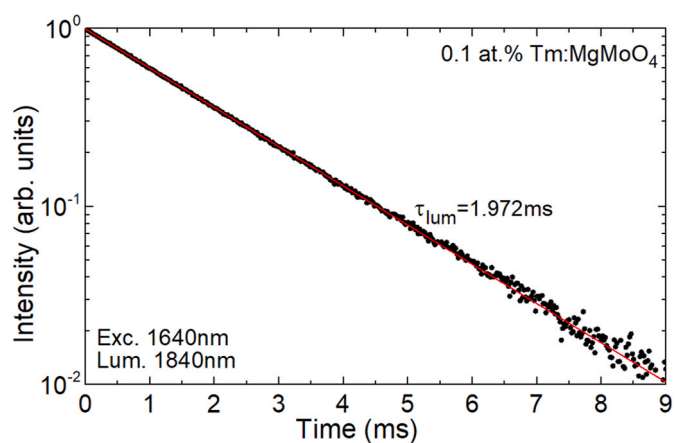


Fig. 12. Luminescence decay curve from the ${}^3\text{F}_4$ state of Tm^{3+} ions in the MgMoO_4 crystal, $\lambda_{\text{exc}} = 1640$ nm, $\lambda_{\text{lum}} = 1840$ nm, red line – single-exponential fit.

excited state τ_{lum} is relatively long, 1.972 ms and it is close to that for $\text{Tm}:\text{MgWO}_4$ ($\tau_{\text{lum}} = 1.93$ ms) [11] and essentially longer than that for Tm^{3+} ions in scheelite-type molybdates ($\tau_{\text{lum}} = 1.1$ ms for $\text{NaLa}(\text{MoO}_4)_2$ [52]). A long lifetime of the upper laser level is favorable for low-threshold laser generation.

4. Conclusions

To conclude, we report on the Czochralski growth, Rietveld structure refinement, thermal, vibronic and spectroscopic properties of a thulium-doped magnesium molybdate, $\text{Tm}^{3+}:\text{MgMoO}_4$, belonging to the crystal family of monoclinic divalent metal mono-tungstates/molybdates, which are currently attracting a lot of attention as laser gain media suitable for high-power/ultrashort-pulse generation. Disordered $\text{Tm}^{3+}:\text{MgMoO}_4$ adopts a monoclinic structure (sp. gr. $C2/m$) being different from that of the ordered $\text{Tm}:\text{MgWO}_4$ crystal (sp. gr. $P2/c$) and featuring two non-equivalent sites for the host-forming Mg^{2+} cations (still, it seems the dopant Tm^{3+} ions predominantly reside in only one type of sites). The difference in the ionic radii and the valence state of Mg^{2+} and Tm^{3+} probably determine the low segregation coefficient of the latter which is expected to be improved when introducing proper charge compensators. Still, the Cz growth attempt was successful for $\text{Tm}^{3+}:\text{MgMoO}_4$ resulting in large-volume transparent crystals with a bright yellow coloration. It seems to be associated with hole centers at molybdenum vacancies and can be eliminated to a great extent by annealing in MoO_3 vapor atmosphere. The thermal conductivity of

$\text{Tm}^{3+}:\text{MgMoO}_4$ at room temperature is moderate ($2.64 \text{ Wm}^{-1}\text{K}^{-1}$) still being much higher than that of disordered tetragonal sodium rare-earth double molybdates.

In terms of spectroscopic properties, Tm^{3+} ions in MgMoO_4 feature (i) broad absorption around 0.8 μm , (ii) smooth and broad emission bands owing to the ${}^3\text{F}_4 \rightarrow {}^3\text{H}_6$ transition extending well above 2 μm thus making this crystal attractive for ultrashort pulse generation, (iii) strongly polarized emission spectra which is a prerequisite for linearly polarized laser emission, (iv) long luminescence lifetime of the ${}^3\text{F}_4$ state and (v) intense and strongly polarized Raman spectra. For achieving laser operation, crystals with higher Tm^{3+} doping levels are necessary.

CRediT authorship contribution statement

Kirill Subbotin: Conceptualization, Methodology, Writing – original draft. **Anatolii Titov:** Investigation. **Denis Lis:** Investigation. **Yulia Zimina:** Writing – original draft. **Yana Didenko:** Investigation. **Ghas-sen Zin Elabedine:** Investigation. **Kirill Ereemeev:** Investigation. **Rosa Maria Solé:** Investigation, Methodology, Writing – review & editing. **Magdalena Aguiló:** Supervision, Funding acquisition. **Pavel Volkov:** Investigation, Writing – original draft. **Pavel Popov:** Investigation. **Elena Chernova:** Investigation. **Francesc Díaz:** Supervision, Funding acquisition. **Patrice Camy:** Supervision, Funding acquisition. **Pavel Loiko:** Conceptualization, Methodology, Writing – review & editing. **Xavier Mateos:** Conceptualization, Supervision, Writing – review & editing.

Declaration of competing interest

The authors declare that they have no known competing financial interests or personal relationships that could have appeared to influence the work reported in this paper.

Data availability

No data was used for the research described in the article.

Acknowledgments

The research was supported by the Ministry of Science and Higher Education of Russia (project No. FSSM-2020-0005). The ICP-AES analysis was done using equipment of the NRC “Kurchatov Institute” — IREA Shared Knowledge Center under financial support by the Russian Federation, represented by the Ministry of Science and Higher Education, agreement No. 075-15-2022-1157 dd. August 16, 2022. Grant PID2019-108543RB-I00 funded by MCIN/AEI/10.13039/501100011033. Grant PECT “Cuidem el que ens uneix”, operation 4 Sensòrica, Act 4 Fotònica” PR15-020174 co-financed by the European Regional Development Fund “ERDF A way of making Europe” through the ERDF Catalonia Operational Programme 2014–2020.

References

- [1] J.M. Cano-Torres, M. Rico, X. Han, M.D. Serrano, C. Cascales, C. Zaldo, V. Petrov, U. Griebner, X. Mateos, P. Koopmann, C. Kränkel, Comparative study of crystallographic, spectroscopic, and laser properties of Tm^{3+} in $\text{NaT}(\text{WO}_4)_2$ ($T = \text{La, Gd, Y, and Lu}$) disordered single crystals, *Phys. Rev. B* 84 (2011) 1–15, 174207.
- [2] V. Petrov, M.C. Pujol, X. Mateos, Ó. Silvestre, S. Rivier, M. Aguiló, R.M. Solé, J. H. Liu, U. Griebner, F. Díaz, Growth and properties of $\text{KLu}(\text{WO}_4)_2$, and novel ytterbium and thulium lasers based on this monoclinic crystalline host, *Laser Photon. Rev.* 1 (2007) 179–212.
- [3] P.V. Klevtsov, R.F. Klevtsova, Polymorphism of the double molybdates and tungstates of mono- and trivalent metals with the composition $\text{M}^{+}\text{R}^{3+}(\text{EO}_4)_2$, *J. Struct. Chem.* 18 (1977) 339–355.
- [4] L. Zhang, W. Chen, J. Lu, H. Lin, L. Li, G. Wang, G. Zhang, Z. Lin, Characterization of growth, optical properties, and laser performance of monoclinic $\text{Yb}:\text{MgWO}_4$ crystal, *Opt. Mater. Express* 6 (2016) 1627–1634.
- [5] L. Zhang, H. Lin, G. Zhang, X. Mateos, J.M. Serres, M. Aguiló, F. Díaz, U. Griebner, V. Petrov, Y. Wang, P. Loiko, E. Vilejshikova, K. Yumashev, Z. Lin, W. Chen, *Crystal*

- growth, optical spectroscopy and laser action of Tm^{3+} -doped monoclinic magnesium tungstate, *Opt Express* 2 (2017) 3682–3693.
- [6] A. Volokitina, S.P. David, P. Loiko, K. Subbotin, A. Titov, D. Lis, R.M. Solé, V. Jambunathan, A. Lucianetti, T. Mocek, P. Camy, U. Griebner, V. Petrov, M. Aguiló, F. Díaz, X. Mateos, Monoclinic zinc monotungstate $\text{Yb}^{3+}, \text{Li}^{+}:\text{ZnWO}_4$: Part II. Polarized spectroscopy and laser operation, *J. Lumin.* 231 (2021) 117811, 1–12.
- [7] V.B. Kravchenko, Crystal structure of the monoclinic form of magnesium tungstate MgWO_4 , *J. Struct. Chem.* 10 (1969) 139–140.
- [8] V.B. Mikhailik, H. Kraus, V. Kapustyanyk, M. Panasyuk, P. Yu, V. Tsybul'skiy, L. Vasylychko, Structure, luminescence and scintillation properties of the MgWO_4 – MgMoO_4 system, *J. Phys. Condens. Matter* 20 (2008) 1–8, 365219.
- [9] P. Loiko, M. Chen, J.M. Serres, L. Zhang, Z. Lin, H. Lin, G. Zhang, Y. Wang, V. Petrov, U. Griebner, S. Dai, Z. Chen, P. Camy, M. Aguiló, F. Díaz, W. Chen, X. Mateos, Spectroscopy and high-power laser operation of monoclinic $\text{Yb}^{3+}:\text{MgWO}_4$ crystal, *Opt. Lett.* 45 (2020) 1770–1773.
- [10] L. Zhang, L. Basyrova, P. Loiko, P. Camy, Z. Lin, G. Zhang, S. Slimi, R.M. Solé, X. Mateos, M. Aguiló, F. Díaz, E. Dunina, A. Kornienko, U. Griebner, V. Petrov, L. Wang, W. Chen, Growth, structure and polarized spectroscopy of monoclinic $\text{Er}^{3+}:\text{MgWO}_4$ crystal, *Opt. Mater. Express* 12 (2022) 2028–2040.
- [11] P. Loiko, J.M. Serres, X. Mateos, M. Aguiló, F. Díaz, L.Z. Zhang, Z.B. Lin, H.F. Lin, G. Zhang, K. Yumashev, V. Petrov, U. Griebner, Y.C. Wang, S.Y. Choi, F. Rotermund, W.D. Chen, Monoclinic $\text{Tm}^{3+}:\text{MgWO}_4$: novel crystal for continuous-wave and passively Q-switched lasers at $\sim 2 \mu\text{m}$, *Opt. Lett.* 42 (2017) 1177–1180.
- [12] L. Zhang, P. Loiko, J.M. Serres, E. Kifle, H. Lin, G. Zhang, E. Vilejshikova, E. Dunina, A. Kornienko, L. Fomicheva, U. Griebner, V. Petrov, Z. Lin, W. Chen, K. Subbotin, M. Aguiló, F. Díaz, X. Mateos, Growth, spectroscopy and first laser operation of monoclinic $\text{Ho}^{3+}:\text{MgWO}_4$ crystal, *J. Lumin.* 213 (2019) 316–325.
- [13] P. Loiko, L. Zhang, J.M. Serres, Y. Wang, M. Aguiló, F. Díaz, Z. Lin, H. Lin, G. Zhang, E. Vilejshikova, E. Dunina, A. Kornienko, L. Fomicheva, V. Petrov, U. Griebner, W. Chen, X. Mateos, Monoclinic $\text{Tm}:\text{MgWO}_4$ crystal: crystal-field analysis, tunable and vibronic laser demonstration, *J. Alloys Compd.* 763 (2018) 581–591.
- [14] L. Zhang, Y. Huang, S. Sun, F. Yuan, Z. Lin, G. Wang, Thermal and spectral characterization of $\text{Cr}^{3+}:\text{MgWO}_4$ – a promising tunable laser material, *J. Lumin.* 169 (2016) 161–164. Part A.
- [15] Y. Wang, W. Chen, M. Mero, L. Zhang, H. Lin, Z. Lin, G. Zhang, F. Rotermund, Y. J. Cho, P. Loiko, X. Mateos, U. Griebner, V. Petrov, Sub-100 fs $\text{Tm}:\text{MgWO}_4$ laser at 2017 nm mode-locked by a graphene saturable absorber, *Opt. Lett.* 42 (2017) 3076–3079.
- [16] E. Cavalli, A. Belletti, M.G. Brik, Optical spectra and energy levels of the Cr^{3+} ions in MWO_4 ($M = \text{Mg}, \text{Zn}, \text{Cd}$) and MgMoO_4 crystals, *J. Phys. Chem. Solid.* 69 (2008) 29–34.
- [17] V.B. Mikhailik, H. Kraus, V. Kapustyanyk, M. Panasyuk, P. Yu, V. Tsybul'skiy, L. Vasylychko, Structure, luminescence and scintillation properties of the MgWO_4 – MgMoO_4 system, *J. Phys. Condens. Matter* 20 (2008) 1–8, 365219.
- [18] L. Li, Y. Huang, L. Zhang, Z. Lin, G. Wang, Growth, mechanical, thermal and spectral properties of $\text{Cr}^{3+}:\text{MgMoO}_4$ crystal, *PLoS One* 7 (2012), e30327.
- [19] V. Bakakin, R. Klevtsova, L. Gaponenko, Crystal structure of magnesium molybdate MgMoO_4 an example of modified closest packing with two types of tetrahedra, *Kristallografiya* 27 (1982) 38–42.
- [20] W. Ran, L. Wang, M. Yang, X. Kong, D. Qu, J. Shi, Enhanced energy transfer from Bi^{3+} to Eu^{3+} ions relying on the criss-cross cluster structure in MgMoO_4 phosphor, *J. Lumin.* 192 (2017) 141–147.
- [21] L.P. Litovskina, Electron paramagnetic resonance of ions of the 3d and 4f groups in single crystals of MgMoO_4 , *J. Struct. Chem.* 7 (1967) 575–577.
- [22] A.A.G. Santiago, M.C. Oliveira, R.A.P. Ribeiro, R.L. Tranquilin, E. Longo, S.R. de Lázaro, F.V. Motta, M.R.D. Bomio, Atomistic perspective on the intrinsic white-light photoluminescence of rare-earth free MgMoO_4 nanoparticles, *Cryst. Growth Des.* 20 (2020) 6592–6603.
- [23] L.G. Uitert, J.J. Rubin, W.A. Bonner, Preparation of single crystals of tungstates and molybdates of a number of divalent metal ions, *J. Am. Ceram. Soc.* 46 (1963) 512, 512.
- [24] L.P. Litovskina, M.L. Meil'man, V.G. Andrianov, N.I. Sergeeva, Electron paramagnetic resonance of Cr^{3+} ions in MgMoO_4 monocrystals, *J. Struct. Chem.* 6 (1966) 615–616.
- [25] D.A. Spasskii, V.N. Kolobanov, V.V. Mikhailin, L.Yu Berezovskaya, L.I. Ivleva, I. S. Voronina, Luminescence peculiarities and optical properties of MgMoO_4 and $\text{MgMoO}_4:\text{Yb}$ crystals, *Opt. Spectra* 106 (2009) 556–563.
- [26] V. Mikhailik, H. Kraus, D. Wahl, M.S. Mykhaylyk, Studies of electronic excitations in MgMoO_4 , CaMoO_4 and CdMoO_4 crystals using VUV synchrotron radiation, *Phys. Status Solidi B* 242 (2005) R17–R19.
- [27] V.B. Mikhailik, H. Kraus, M. Itoh, D. Iri, M. Uchida, Radiative decay of self-trapped excitons in CaMoO_4 and MgMoO_4 crystals, *J. Phys. Condens. Matter* 17 (2005) 7209–7218.
- [28] K.A. Subbotin, Y.S. Didenko, P.A. Popov, A.I. Titov, D.A. Lis, S.K. Pavlov, Y. I. Zimina, K.V. Kuleshova, Growth, thermal conductivity and spectroscopic properties of $\text{Nd}:\text{MgMoO}_4$ laser crystal, in: *International Conference Laser Optics, IEEE*, 2022, pp. ThR1–p39, <https://doi.org/10.1109/ICLO54117.2022.9840162>.
- [29] G. Han, Z. Xiao-Bin, C. Wen-Ting, Y. Zhi-Feng, P. Jian-Fu, L. Ling-Yun, Y. Yan, Optical spectroscopic properties of Yb^{3+} -doped MgMoO_4 crystal grown by the TSSG method, *Chin. J. Struct. Chem.* 36 (2017) 631–639.
- [30] M. Morishita, Y. Kinoshita, A. Nozaki, H. Yamamoto, Thermodynamic properties for MMoO_4 ($M = \text{Mg}, \text{Sr}$ and Ba) as the end-members of the yellow phases formed in the nuclear fuel waste glasses, *Appl. Geochem.* 98 (2018) 310–320.
- [31] H. Koç, O. Köse, E. Eser, Low-temperature heat capacities for EMoO_4 ($E = \text{Mg}, \text{Sr}, \text{Ba}$) substances formed in nuclear fuel waste glasses, *Prog. Nucl. Energy* 143 (2022), 104054.
- [32] M. Gancheva, T. Rojac, R. Jordanova, I. Piroeva, P. Ivanov, Structural and optical properties of MgMoO_4 prepared by mechanochemical technique, *Ceram. Int.* 48 (2022) 17149–17156.
- [33] C.S. Xavier, A.P. de Moura, E. Longo, J.A. Varela, M.A. Zaghete, Synthesis and optical property of MgMoO_4 crystals, *Adv. Mater. Res.* 975 (2014) 243–247.
- [34] L. Zhang, W. He, K. Shen, Y. Liu, S. Guo, Controllable synthesis of hierarchical MgMoO_4 nanosheet-arrays and nano-flowers assembled with mesoporous ultrathin nanosheets, *J. Phys. Chem. Solid.* 115 (2018) 215–220.
- [35] M. Amberg, J.R. Günter, H. Schmalle, G. Blasse, Preparation, crystal structure, and luminescence of magnesium molybdate and tungstate monohydrates, $\text{MgMoO}_4 \cdot \text{H}_2\text{O}$ and $\text{MgWO}_4 \cdot \text{H}_2\text{O}$, *J. Solid State Chem.* 77 (1988) 162–169.
- [36] P. Du, J.S. Yu, Photoluminescence and cathodoluminescence properties of Eu^{3+} ions activated AMoO_4 ($A = \text{Mg}, \text{Ca}, \text{Sr}, \text{Ba}$) phosphors, *Mater. Res. Bull.* 70 (2015) 553–558.
- [37] L.-Y. Zhou, J.-S. Wei, L.-H. Yi, F.-Z. Gong, J.-L. Huang, W. Wang, A promising red phosphor $\text{MgMoO}_4:\text{Eu}^{3+}$ for white light emitting diodes, *Mater. Res. Bull.* 44 (2009) 1411–1414.
- [38] J.D. Kim, S. Cho, Optical properties of $\text{MgMoO}_4:\text{Dy}^{3+}, \text{Eu}^{3+}$ phosphors prepared with different Eu^{3+} molar ratios, *J. Korean Inst. Electr. Electron. Mater. Eng.* 29 (2016) 186–191.
- [39] W. Ran, L. Wang, M. Yang, X. Kong, D. Qu, J. Shi, Enhanced energy transfer from Bi^{3+} to Eu^{3+} ions relying on the criss-cross cluster structure in MgMoO_4 phosphor, *J. Lumin.* 192 (2017) 141–147.
- [40] J.E. Miller, N.B. Jackson, L. Evans, A.G. Sault, M.M. Gonzales, The formation of active species for oxidative dehydrogenation of propane on magnesium molybdates, *Catal. Lett.* 58 (1999) 147–152.
- [41] L.E. Cadus, M.C. Abello, M.F. Gomez, J.B. Rivarola, Oxidative dehydrogenation of propane over $\text{Mg}-\text{Mo}-\text{O}$ catalysts, *Ind. Eng. Chem. Res.* 35 (1996) 14–18.
- [42] P.A. Popov, A.A. Sidorov, E.A. Kul'chenkov, A.M. Anishchenko, I.C. Avetissov, N. I. Sorokin, P.P. Fedorov, Thermal conductivity and expansion of PbF_2 single crystals, *Ionics* 23 (2017) 233–239.
- [43] G.M. Kuz'micheva, V.B. Rybakov, K.A. Subbotin, E.V. Zharikov, D.A. Lis, O. Zaharko, D.A. Nikolaev, V.G. Senin, *Russ. J. Inorg. Chem.* 57 (2012) 1128.
- [44] V.F. Tarasov, A.A. Sukhanov, E.V. Zharikov, K.A. Subbotin, D.A. Lis, EPR spectroscopy of impurity ytterbium ions in synthetic forsterite single crystals, *Appl. Magn. Reson.* 53 (2022) 1211–1226.
- [45] K.A. Subbotin, A.I. Titov, S.K. Pavlov, P.A. Volkov, V.V. Sanina, D.A. Lis, O.N. Lis, Y.I. Zimina, Y.S. Didenko, E.V. Zharikov, Effect of Li^{+} codoping on the mechanical strength of $\text{Yb}:\text{ZnWO}_4$ single crystals, *J. Cryst. Growth* 582 (2022), 126498.
- [46] A.A. Blistanov, B.I. Galagan, B.I. Denker, L.I. Ivleva, V.V. Osiko, N.M. Polozkov, Yu.E. Sverchkov, Spectral and lasing characteristics of $\text{CaMoO}_4:\text{Nd}^{3+}$ single crystals, *Quant. Electron.* 19 (1989) 747–748.
- [47] S.C. Abrahams, Crystal structure of the transition-metal molybdates and tungstates. III. Diamagnetic α - ZnMoO_4 , *J. Chem. Phys.* 46 (1967) 2052–2063.
- [48] M.N. Coelho, P.T.C. Freire, M. Maczka, C. Luz-Lima, G.D. Saraiva, W. Paraguassu, A.G. Souza Filho, P.S. Pizani, High-pressure Raman scattering of MgMoO_4 , *Vib. Spectrosc.* 68 (2013) 34–39.
- [49] V.M. Zhukovskii, E.V. Tkachenko, T.A. Rakova, *Zhurnal Neorganicheskoi Khimii* 15 (1970) 3326–3328.
- [50] P.A. Popov, S.A. Skrobov, E.V. Zharikov, D.A. Lis, K.A. Subbotin, L.I. Ivleva, V. N. Shlegel, M.B. Kosmyna, A.N. Shekhovtsov, Investigation of the thermal conductivity of tungstate crystals, *Crystallogr. Rep.* 63 (2018) 111–116.
- [51] P.J. Miller, The Raman spectra of MgMoO_4 , *Spectrochim. Acta: Molec. Spectr.* 27 (1971) 957–960.
- [52] Yu.K. Voron'ko, E.V. Zharikov, D.A. Lis, A.V. Popov, V.A. Smirnov, K.A. Subbotin, M.N. Khromov, V.V. Voronov, Growth and spectroscopic studies of $\text{NaLa}(\text{MoO}_4)_2:\text{Tm}^{3+}$ crystals: a new promising laser material, *Opt. Spectra* 105 (2008) 538–546.